ACS Photonics

Article

pubs.acs.org/journal/apchd5

Tuning the First Hyperpolarizabilities of Boron Nitride Nanotubes

Jia Gu,[†] Yuan-Qi Le,[†] Yang-Yang Hu,[†] Wei-Qi Li,*[,‡] and Wei Quan Tian*[,†]

[†]State Key Laboratory of Urban Water Resource and Environment, Institute of Theoretical and Simulational Chemistry, Academy of Fundamental and Interdisciplinary Sciences, Harbin Institute of Technology, Harbin, 150080, People's Republic of China

[‡]Department of Physics, Harbin Institute of Technology, Harbin, 150001, People's Republic of China

Supporting Information

ABSTRACT: Various carbon-substituted boron nitride (8,0) and (4,4) nanotubes are designed for application as nonlinear optical materials. The structure and first (static and frequency-dependent) hyperpolarizabilities of these boron nitride nanotubes are predicted. The substitution of carbon in the boron nitride nanotube clip significantly enhances the first hyperpolarizabilities by up to several orders of magnitude. The doping pattern of the carbon circle and π electron conjugation are crucial in determining the large first hyperpolarizabilities of these nanotubes.

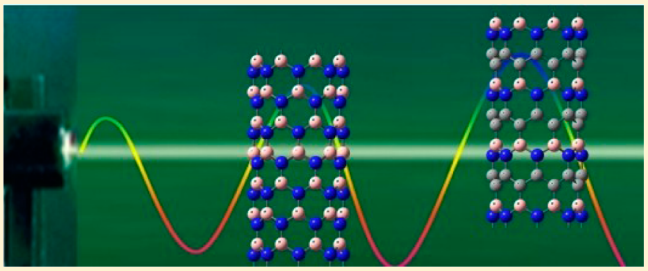

KEYWORDS: *carbon-substituted boron nitride nanotubes, first hyperpolarizability, frequency dispersion, charge transfer based electronic excitation*

Nonlinear optical (NLO) materials have attracted increasing attention due to their potential important applications, e.g., laser tuning, frequency conversion, all-optical switches, signal processing, optical communication, information security, optical data storage processing, and biological imaging.[1,2] Minerals,[3] inorganic oxides,[4] semiconductors,[5] atomic clusters,[6] organometallic compounds,[7] and metal complexes[8−11] have been explored for these applications. Nanotubes could be potential NLO materials due to their unique structures and properties.

Carbon nanotubes (CNTs) could be semiconducting or metallic depending on their chirality[12] with possible exceptions of CNTs (4,0) and (5,0).[13] On the other hand, boron nitride nanotubes (BNNTs) are electric insulators (or wide-gap semiconductors) with band gaps of about 5.5 eV[14] in spite of chirality and their tube diameter.[15] BNNT was predicted theoretically[16] before the experimental synthesis of single- and multiple-wall tubes.[17] The combination of BNNTs and CNTs (BCNNTs) could have some new properties due to the large property differences between BNNTs and CNTs,[18,19] and such combinations were the targets in the synthesis of nanotubes with desired properties.[20−25] The hybridized nanotubes with zigzag conformations may be semiconducting[23] with good thermal stability. The band gaps of hybridized armchair nanotubes [$C_{0.5}(BN)_{0.5}$] do not change with the radius of the tubes.[24] The electronic structures of certain BCNNTs with proper hybridization, e.g., BC_2N, depend on the radii or chiralities of the tubes,[25] providing new opportunities for the design of electronic devices.

First-principles calculations predict large second-order nonlinear optical properties for BNNTs[26] and possible applications of BN-doped carbon nanotubes in NLO devices.[27] The NLO properties of zigzag BNNTs were predicted to converge to those of a hexagonal-BN sheet.[28] The bonding pattern of C with BN and the composition dictate the electronic structure of BCNNTs,[23−25] and the charge distributions have large effects on the NLO properties[29] of these tubes as well. The polarities, polarizabilities, and the second hyperpolarizabilities of armchair BCNNTs are significantly enhanced[30] with respect to those of BNNTs. However, hybridization of C with BN has little effect on the first hyperpolarizabilities, as predicted by a finite field model.[30] Thus, the correlation of the NLO properties with the hybridization in BCNNTs needs further exploration.

The structure and NLO properties of three types of zigzag (8,0) and armchair (4,4) BCNNTs and two hydrogenated zigzag BCNNTs (as shown in Figure 1) are investigated to provide information for the syntheses and applications of BNNT-based materials. The doping patterns of carbon in BNNTs in the present work are different from those of previous works. The C-BN heteronanotubes[23,24] have carbon atoms doped as a carbon ribbon along the nanotubes. Only "half/half" doping of carbon circles [similar to (8,0) BCNNT *c* in Figure 1] was studied with the elongation method.[30] Carbon circles are doped in the (8,0) and (4,4) BNNTs in various ways in the present work. Carbon circles could serves as π conjugation bridges isolating the polar BN circles to produce multiple local BN dipoles in order to enhance the NLO properties of these materials. Advances in synthetic techniques[31] make these nanotubes possible.

Received: February 19, 2014
Published: September 15, 2014

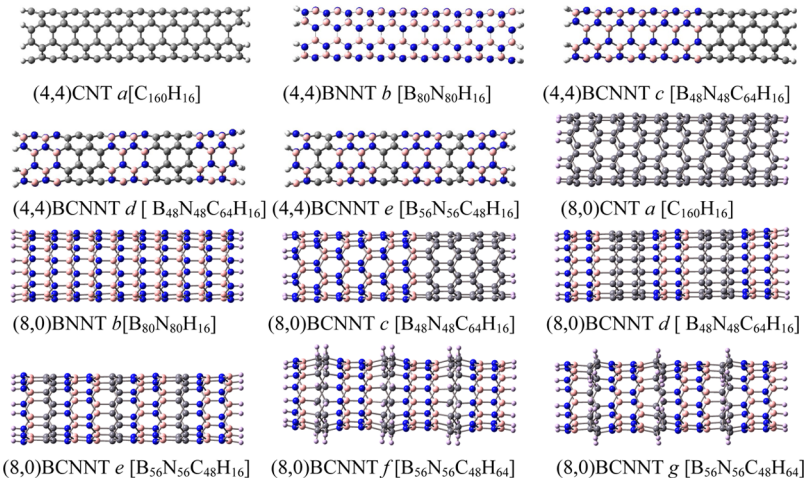

Figure 1. Structures of (4,4) and (8,0) carbon nanotubes (CNTs), boron nitride nanotube (BNNTs), and carbon-doped boron nitride nanotubes (BCNNTs) clips. Atoms in gray are carbon, blue are nitrogen, and pink are boron.

Table 1. Total Energy, $\Delta E = E[n(8,0)] - E[n(4,4)]$ (n = *a*, *b*, *c*, *d*, *e*), Lowest Vibrational Frequency (LVF), Dipole Moments, Energies of the Highest Occupied Molecular Orbital [E(HOMO)] and the Lowest Unoccupied Molecular Orbital [E(LUMO)], and Energy Gap (E_{gap}) between the HOMO and LUMO of Carbon Nanotube (8,0) CNT *a*, Boron Nitride Nanotube (8,0) BNNT *b*, Carbon-Doped Boron Nitride Nanotube Clips BCNNT (*c* to *g*), (4,4) CNT *a*, (4,4) BNNT *b*, and (4,4) BCNNT (*c* to *e*), Predicted by B3LYP/6-31G(d,p)[a]

	total energy (au)	ΔE (eV)	LVF (cm^{-1})	dipole (D)	E_{HOMO} (eV)	E_{LUMO} (eV)	E_{gap}(eV)	λ_{max} (nm)	β_0 ($\times 10^{-30}$esu)
(8,0) CNT *a*	−6105.565064	−3.55	64.4	0.0	−4.24	−1.55	2.70		
(4,4) CNT *a*	−6105.434350		64.0	0.004	−4.12	−3.02	1.10		
(8,0) BNNT *b*	−6386.095968	−4.94	58.4	11.4	−6.40	−1.29	5.11	198.1	77.99
(4,4) BNNT *b*	−6385.914290		56.2	0.01	−6.50	−0.35	6.15	211.5	0.15
(8,0) BCNNT *c*	−6273.761298	−4.71	59.4	4.5	−4.16	−3.75	0.41	5203.7	1871.15
(4,4) BCNNT *c*	−6273.588097		58.1	1.7	−4.32	−2.55	1.76	919.5	467.17
(8,0) BCNNT *d*	−6273.127037	−1.14	65.7	25.4	−3.32	−3.05	0.27	996.7	1053.89
(4,4) BCNNT *d*	−6273.084962		58.3	0.0	−4.86	−1.93	2.93	525.6	0.22
(8,0) BCNNT *e*	−6301.005518	−3.93	63.8	20.2	−3.60	−2.61	1.00	471.4	486.79
(4,4) BCNNT *e*	−6300.860923		57.5	0.4	−4.42	−2.34	2.08	646.7	32.64
(8,0) BCNNT *f*	−6328.835136		38.7	37.9	−5.08	−0.38	4.70	201.5	104.93
(8,0) BCNNT *g*	−6328.726616		69.1	39.1	−5.47	−0.99	4.48	201.7	106.33

[a]The wavelength (λ_{max}) of the lowest electronic excitation is predicted by ZINDO, and the static first hyperpolarizability (β_0) is predicted with the sum-over-states model. Energies are corrected with zero-point vibrational energy.

MODELS AND COMPUTATIONAL DETAILS

The (8,0) and (4,4) single-wall nanotube clips saturated with hydrogen at their two ends are chosen as models, and eight BCNNT clips are designed (Figure 1). Their structures are optimized through density functional theory[32−34] based method B3LYP[35,36] with 6-31G(d,p)[37,38] basis sets as implemented in the Gaussian03 package.[39] Carbon is doped in the BNNTs in the form of a cycle to produce half/half BCNNTs and alternately doped BCNNTs. The carbon atoms in the BCNNTs [(8,0) BCNNT *f* and *g*] are saturated with hydrogens (on the outside of the nanotube *f* and on both sides of the nanotube *g* as shown in Figure 1) to evaluate the effect of π conjugation on the electronic structure and NLO properties of nanotubes. Such saturation of the π conjugation is not explored for the (4,4) BCNNTs due to the high strain of the tube caused by the smaller radius and by the BN bonding perpendicular to the tube direction. Another possibility for hydrogen saturation of BCNNTs is bonding of hydrogen with B and N atoms, but this will not be investigated in the present work. All these structures are minima on the potential energy surface according to vibrational frequency calculations. Other various doping patterns were also explored. However, no stable structures were obtained.

The electronic spectra of these systems are predicted with ZINDO,[40] and the first hyperpolarizabilities are predicted with the sum over states (SOS) model,[41−44]

$$\beta_{ijk}(\omega_s;\ \omega_1,\ \omega_2)_{m,n} = \hbar^{-2} \sum P_{ijk} \sum_{\substack{m,n \\ (\neq g)}} \frac{r^i_{gm} \bar{r}^j_{mn} r^k_{ng}}{(\omega_{mg} - \omega_\sigma + i\Gamma_m)(\omega_{ng} - \omega_1 + i\Gamma_n)}$$

$\omega_\sigma = \sum \omega_i$ is the sum of external fields ω_i. $\bar{r}^j_{mn} = \langle m|\mu^j|n\rangle - \langle g|\mu^j|g\rangle\delta_{mn}$ is the dipole fluctuation. The orientation averaged total first hyperpolarizability is reported in the present work, although it does not correspond to a physical observable. The magnitude of the averaged total first hyperpolarizability reflects the strength of response of a system to an external field.

Due to the size of the nanotube clips, only configuration interaction singles (CIS) is employed for electronic spectra and the first hyperpolarizability predictions. A total of 45 occupied

dx.doi.org/10.1021/ph500059c | ACS Photonics 2014, 1, 928−935

and 45 unoccupied frontier molecular orbitals were included in the CIS calculations. This active space predicts the electronic excitation up to 12.0 eV, thus including contributions of the most important electronic excitations to NLO properties. ZINDO-SOS made similar predictions of the first hyperpolarizabilites of a series of chiral molecules to those from the finite field method combined with density functional theory based methods.[45] This scheme has been used extensively in nonlinear optical material simulations.[46] The polarizabilities of CNTs predicted from the SOS scheme vary linearly with those from response theory.[47] The difference in the predicted polarizabilities of CNTs by SOS from those by the coupled perturbed Kohn–Sham scheme was ascribed to wave function relaxation, and the predicted polarizabilities can be correlated through scaling factors.[48]

RESULTS AND DISCUSSION

Structures. The structures and relevant electronic properties of these nanotube clips are shown in Figure 1 and listed in Table 1. With the same size, the (8,0) CNT *a* ($C_{160}H_{16}$) is 3.55 eV more stable than the (4,4) CNT *a*, in the same order of relative stability as predicted for armchair and zigzag CNTs.[48] This is the similar case for all (8,0) and (4,4) BNNTs and BCNNTs; that is, all (8,0) nanotubes are more stable than their (4,4) counterparts. The strain due to the smaller diameter and the BN bonding perpendicular to the tube direction causes such instability in (4,4) nanotubes. Because of the radial distribution of the BN pair in the (4,4) nanotubes, all (4,4) nanotubes have a small dipole moment. Thus, this present work focuses on the discussion of the NLO properties of (8,0) nanotubes, although the NLO properties of (4,4) nanotubes will be discussed for comparison with those of (8,0) nanotubes [electronic spectra and NLO properties of (4,4) nanotubes are provided in the Supporting Information].

(8,0) CNT *a* has an energy gap of 2.70 eV between the highest occupied molecular orbital (HOMO) and the lowest unoccupied molecular orbital (LUMO), larger than the gap predicted with the HSE06 functional.[49] (8,0) BNNT *b* ($B_{80}N_{80}H_{16}$) has a HOMO–LUMO gap of 5.11 eV and a dipole moment of 11.4 D. In (8,0) BCNNT *c* ($B_{48}N_{48}C_{64}H_{16}$), half of the tube is carbon circles and the other half is BN circles with boron atoms bonded to carbon atoms. This half/half graft brings about a small HOMO–LUMO energy gap of 0.41 eV and a dipole moment of 4.5 D. Optimization of an isomer with nitrogen bonded to carbon has not yet been achieved.

(8,0) BCNNT *d* ($B_{48}N_{48}C_{64}H_{16}$) has alternate doping of two layers of carbon nanorings between two layers of BN nanorings. This alternate doping destabilizes this BCNNT by 17.66 eV with respect to (8,0) BCNNT *c*. This destabilization might be due to the bonding between the carbon circles and the BN circles, which increases the strain of the tube. This alternate doping of carbon rings brings about a large dipole moment of 25.4 D. This BCNNT has an even smaller HOMO–LUMO energy gap (0.27 eV). A single layer of carbon circles is inserted between two layers of BN circles [(8,0) BCNNT *e* ($B_{56}N_{56}C_{48}H_{16}$)] to check the effect of the carbon circles on the electronic structure of the nanotube. The HOMO–LUMO energy gap of (8,0) BCNNT *e* is 1.00 eV, and the dipole moment is 20.2 D. The net charge on carbon atoms in BCNNTs is relatively small, and the carbon circles serve as a bridge for π conjugation, as revealed by the charge distribution of these nanotube clips (Figure S1).

The sp^3-hybridized carbon atoms disrupt the π conjugation of the BN circles and the molecular orbital energies of the newly formed CH bonds move downward into the bands of occupied molecular orbitals, thus resulting in larger HOMO–LUMO energy gaps in (8,0) BCNNTs *f* (4.70 eV) and *g* (4.48 eV). The hydrogenation of carbon atoms in BCNNT *f* releases 2.85 eV energies, while only 0.06 eV energies are released by the hydrogenation in (8,0) BCNNT *g*; that is, BCNNT *f* is 2.79 eV more stable than BCNNT *g*. The bonding of hydrogen atoms to carbon atoms on the inner side of the tube does not stabilize the nanotube, and the small radius of the nanotube is not large enough for the optimal sp^3 bonding of the carbon atoms, thus not releasing much strain in BCNNT *g*. The isolation of π electrons in the BN circles and polar charge distribution lead to large dipole moments in BCNNTs *f* (37.9 D) and *g* (39.1 D).

Electronic Spectra and the Static First Hyperpolarizability. Figure 2 depicts the electronic spectra (the evolution of the static first hyperpolarizability with the electronic spectra is shown in Figure S2) of all (8,0) nanotube clips investigated. In (8,0) BNNT *b*, there are four major absorption peaks, at 6.26 eV (198.1 nm), 6.74 eV (184.0 nm), 7.28 eV (170.3 nm), and 7.35 eV (168.7 nm), with the strongest peak at 6.74 eV. The absorption with the longest wavelength occurs at 6.26 eV, involving excitations with a mixture of vertical and charge transfer based excitations (relevant molecular orbitals are in Figure S3). The absorption peak at 6.74 eV includes contributions from many electronic excitations; however, no single electronic transition has a dominant contribution. This electronic excitation has a major contribution, over 50.0 × 10^{-30} esu, to the static first hyperpolarizability (77.99 × 10^{-30} esu) of this BNNT clip. On the other hand, (4,4) BNNT *b* has a very small static first hyperpolarizability (0.15 × 10^{-30} esu).

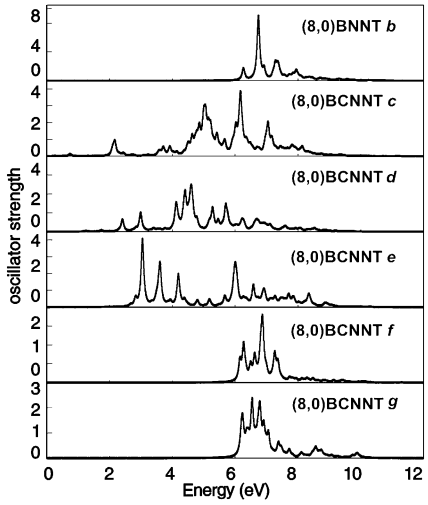

Figure 2. Electronic spectra of (8,0) nanotube clips.

The electronic spectra of (8,0) BCNNT *c* below 6.0 eV are similar to those of (8,0) CNT *a* (as shown in Supporting Information Figure S4), and those above 8.0 eV are similar to those of (8,0) BNNT *b*. There are six absorption bands, at about 0.74 eV (1675.5 nm), 2.17 eV (571.4 nm), 4.63 eV (267.8 nm), 5.06 eV (245.0 nm), 6.17 eV (200.9 nm), and 7.05 eV (175.9 nm), with the strongest peak at 6.17 eV. The lowest electronic excitation occurs at 0.24 eV (5023.7 nm) in the infrared region with a charge transfer based transition from the

dx.doi.org/10.1021/ph500059c | ACS Photonics 2014, 1, 928–935

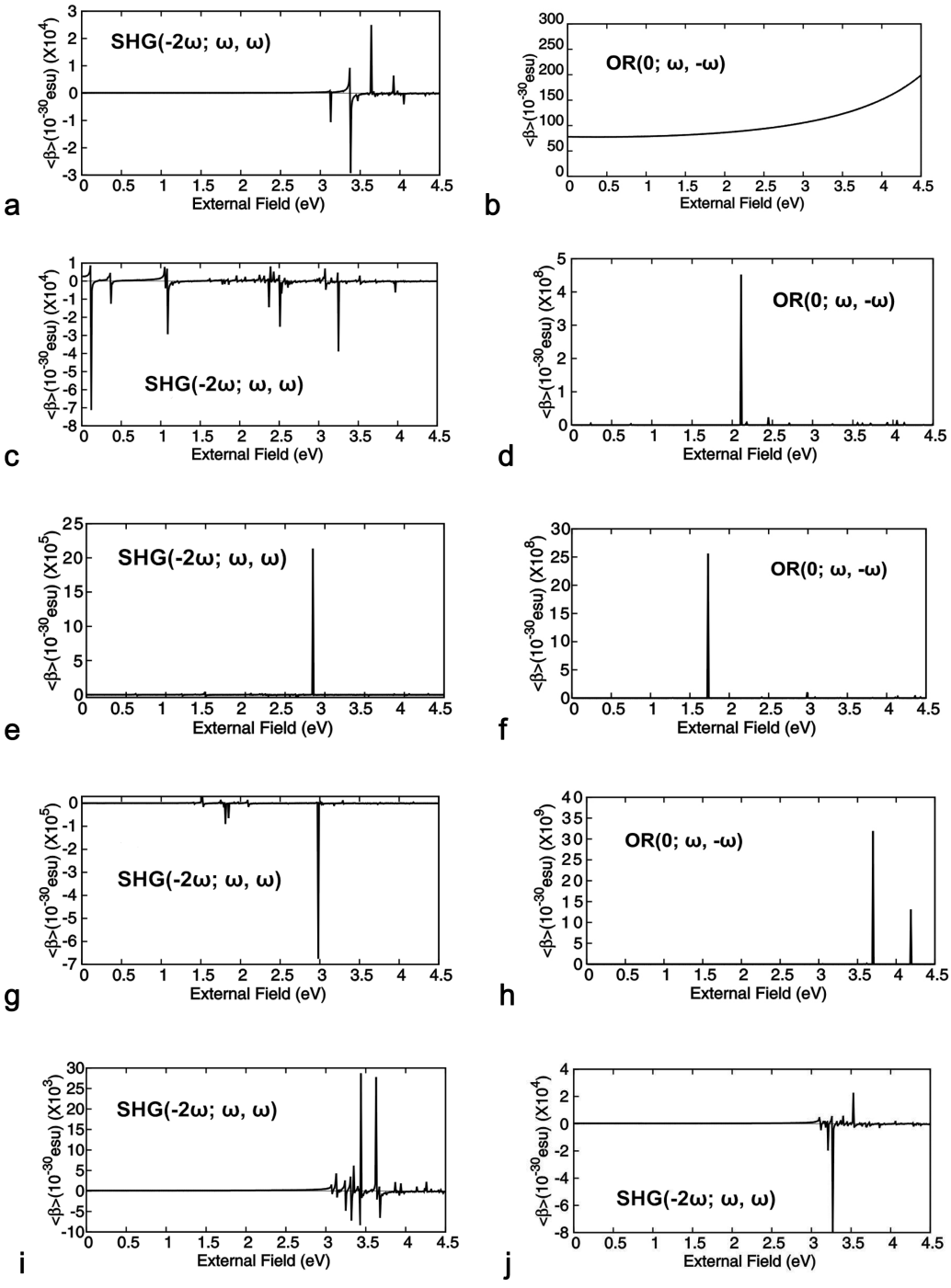

Figure 3. Frequency dependence of the first hyperpolarizabilities of (8,0) BNNT and (8,0) BCNNTs. (a) [BNNT *b*]; (b) [BNNT *b*]; (c) [BCNNT *c*]; (d) [BCNNT *c*]; (e) [BCNNT *d*]; (f) [BCNNT *d*]; (g) [BCNNT *e*]; (h) [BCNNT *e*]; (i) [BCNNT *f*]; (j) [(BCNNT *g*].

HOMO (bonding between the BN circles and carbon circles) to the LUMO (the π orbital at the carbon open end). Such low-energy excitation also occurs in BN-doped fullerenes.[50] The absorption at 0.74 eV (1683.9 nm) involves charge transfer based transition. The first electronic excitation around 0.24 eV makes a dominant contribution (over 1300.0×10^{-30} esu) to the static first hyperpolarizability. The electronic excitations around 2.17 eV (relevant molecular orbitals are in Figure S5) also make significant contributions (over 100.0×10^{-30} esu) to the static first hyperpolarizability as well. Charge transfer (from the middle of the tube to the carbon end) based electronic excitations make dominant contributions to the static first hyperpolarizability of BCNNT *c*. This type of graft of carbon circles to (4,4) BNNT also enhances the static first hyperpolarizability (467.17×10^{-30} esu) of (4,4) BNNT *c*, though smaller than that in (8,0) BNNT *c*.

The alternate doping of carbon circles and BN circles in (8,0) BCNNT *d* destabilizes the system and modifies the geometric and electronic structures. The frontier MOs essentially localize at the junction between the BN and carbon circles in (8,0) BCNNT *d*, as shown in Figure S6. Such destabilization (causing an energy increase of the occupied orbitals) by the alternate doping leads to the overall red shift of major absorption peaks in (8,0) BCNNT *d*. There are five

dx.doi.org/10.1021/ph500059c | ACS Photonics 2014, 1, 928−935

major absorption bands in the electronic spectra of (8,0) BCNNT *d*, located around 2.41 eV (514.5 nm), 2.99 eV (414.7 nm), 4.11 eV (301.7 nm), 4.13 eV (300.2 nm), and 4.41 eV (281.1 nm), with the strongest absorption at 4.41 eV. All these excitations mainly involve charge transfer based transition and partially vertical excitations, as manifested by the MOs shown in Figure S6. The lowest dipole-allowed excitation occurs at 1.24 eV (996.7 nm), and it contributes about 100.0×10^{-30} esu to the static first hyperpolarizability of the system. The electronic excitations below 5.0 eV have a dominant contribution (about 800.0×10^{-30} out of 1053.0×10^{-30} esu), with the largest contribution (over 250.0×10^{-30} esu) from the electronic excitation at 2.99 eV. The static first hyperpolarizability of (4,4) BCNNT *d* is only 0.22×10^{-30} esu.

The lowest electronic excitation occurs at 2.63 eV (471.4 nm) with very weak oscillator strength in (8,0) BCNNT *e*. There are three major absorption peaks, at 3.05 eV (406.5 nm), 3.61 eV (343.4 nm), and 4.19 eV (295.9 nm), below 5.0 eV, as shown in Figure 2. The charge transfer based transitions from one end to the other end of the tube are responsible for the absorption peak at 3.05 eV (as shown in Figure S7). Another major electronic excitation occurs at 6.01 eV (206.3 nm) and is essentially vertical excitation of the C π electrons. These electronic excitations make a dominant contribution to the static first hyperpolarizability of the system, with the largest contribution (over 150.0×10^{-30} esu) from the strongest absorption at 3.05 eV. All the MOs (in Figure S7) involved in the major electronic excitations have contributions from carbon circles. (4,4) BCNNT *e* has a much smaller static first hyperpolarizability (32.64×10^{-30} esu). The evolutions of the static first hyperpolarizability with the electronic spectra of (4,4) nanotubes are shown in Figure S8.

The saturation of the carbon circles in (8,0) BCNNTs *f* and *g* modifies their electronic structure, thus affecting the electronic excitations as seen in Figure 2. These two isomers have similar electronic spectra and MOs; for example, there is no dipole-allowed electronic excitation below 6.0 eV. The major electronic excitations are in the range from 6.0 to 8.0 eV and are mixtures of vertical and charge transfer based excitations. These two isomers have similar static first hyperpolarizabilies (about 100.0×10^{-30} esu) and similar evolution with electronic spectra.

The doping patterns of carbon circles in BNNT have significant effects on the electronic properties of the systems. The half/half grafted (8,0) BCNNT *c* has a new feature at the junction besides keeping those features of a carbon nanotube and a BNNT. It has the smallest dipole moment among these BCNNTs. (8,0) BCNNTs *c* and *d* have the smallest HOMO−LUMO energy gaps among all BCNNTs, and (8,0) BCNNT *c* has the lowest dipole-allowed electronic excitation (with relatively large oscillator strength) at 5203.7 nm in the infrared region. The lowest dipole-allowed electronic excitations of (8,0) BCNNTs *d* and *e* with carbon π conjugation also are at long wavelengths. (8,0) BCNNTs *f* and *g* have the largest dipole moments due to the isolation of π conjugation and the polar nature of the BN pairs.

Such electronic features of those BCNNTs lead to different static first hyperpolarzabilities. Due to the small HOMO−LUMO energy gap and dipole-allowed electronic excitations with low excitation energies, BCNNT *c* has the largest static first hyperpolarzability followed by BCNNTs *d* and *e*. The static first hyperpolarzabilities of BCNNTs *f* and *g* are close to that of BNNT *b*. The electronic spectra and the static first hyperpolarzabilities of these BCNNTs reveal the role of carbon doping and π conjugation.

Frequency Dispersion of the First Hyperpolarizabilities. *(8,0) BNNT b.* The frequency dispersion (second-harmonic generation and optical rectification) of the first hyperpolarizability was calculated to study the second-order NLO response of those BCNNTs to external fields up to 4.50 eV. Figure 3 depicts the evolution of the second-harmonic generation (SHG) $(-2\omega;\ \omega,\ \omega)$ (Figure 3a) and optical rectification (OR) $(0;\ \omega,\ -\omega)$ (Figure 3b) of (8,0) BNNT *b* with external field. There are four strong responses of SHG in external fields from 3.00 to 4.00 eV, with the strongest one at 3.38 eV (366.9 nm). The SHG response switches from a positive peak to a negative peak around 3.38 eV. Such a phenomenon was predicted in zigzag BNNTs.[51]

The strong response of SHG at an external field of 3.64 eV (340.7 nm) is due to the electronic excitation at 7.28 eV (170.5 nm) (Figure S3) (with a contribution of over 25000.0×10^{-30} esu). The electronic excitation at 7.28 eV has no single-electron transition with dominant contribution in the configuration interactions. On the other hand, the response of OR increases with the strength of the external field monotonically as shown in Figure 3b. (4,4) BNNT *b* has a much weaker SHG response around 3.4 eV (364.7 nm) (about 60.0×10^{-30} esu), and its OR responses to external fields are similar to but much weaker than those of (8,0) BNNT *b* (Figure S9).

(8,0) BCNNT c. In the presence of an external field, (8,0) BCNNT *c* [$B_{48}N_{48}C_{64}H_{16}$ with half/half graft] has several strong responses [0.12 eV (10333.3 nm or 967.7 cm^{-1}), 0.37 eV (3351.4 nm or 2984.2 cm^{-1}), 1.09 eV (1137.6 nm), 2.37 eV (523.2 nm), 2.51 eV (494.0 nm), and 3.25 eV (381.5 nm)] in the SHG process, with the strongest one at 0.12 eV (Figure 3c). The strongest SHG response reaches 70000.0×10^{-30} esu in the infrared region (967.7 cm^{-1}), and it is ascribed to the HOMO−LUMO charge transfer based electronic excitation at 0.24 eV (5203.7 nm, or 1921.7 cm^{-1}) (Figure S5a). The strong SHG responses of this system make this half/half doped BCNNT a potential NLO material in the visible and infrared regions. In the infrared region, the NLO response could have contributions from vibrational contribution, e.g., through vibronic coupling. In the external fields from 0.0 to 4.5 eV, the system has a very strong OR response (over $4.5 \times 10^{8} \times 10^{-30}$ esu) at 2.11 eV (587.6 nm) due to the resonant (electronic excitation at 2.11 eV) interaction of the system with the external field (Figure 3d). This absorption peak (2.11 eV) is a mixture of vertical and charge transfer based excitations in the carbon part of the tube (Figure S5b). (4,4) BCNNT *c* has a strong SHG response ($1.5 \times 10^{5} \times 10^{-30}$ esu) at 1.8 eV (688.9 nm) and a strong OR response ($1.5 \times 10^{8} \times 10^{-30}$ esu) at 2.60 eV (476.9 nm) (Figure S9).

(8,0) BCNNT d. In the SHG process, (8,0) BCNNT *d* [$B_{48}N_{48}C_{64}H_{16}$, with carbon alternately doped] has a strong response (over $2.0 \times 10^{6} \times 10^{-30}$ esu) at 2.84 eV(436.6 nm), as shown in Figure 3e. At this field, the electronic excitation at 5.70 eV (217.5 nm) has a dominant contribution to the SHG response. These electronic transitions involve charge transfer from the BN belt to the carbon belt and vice versa, as shown in Figure S6a. A strong response (over $2.5 \times 10^{9} \times 10^{-30}$ esu) occurs at 1.72 eV (720.9 nm) in the OR process, as shown in Figure 3f. The electronic excitation (at 1.72 eV) with dominant contribution to this strong OR response has relatively weak oscillator strength, and the resonance of this electronic excitation with external field leads to such a strong OR

dx.doi.org/10.1021/ph500059c | ACS Photonics 2014, 1, 928−935

response. A relatively strong SHG response (200.0×10^{-30} esu) at 1.72 eV (720.9 nm) occurs in the response of (4,4) BCNNT *d* to an external field, and (4,4) BCNNT *d* has an OR response ($9.4 \times 10^{5} \times 10^{-30}$ esu) around 4.30 eV (288.4 nm) (Figure S9).

(8,0) BCNNT e. (8,0) BCNNT *e* has a strong SHG response (over $6.0 \times 10^{5} \times 10^{-30}$ esu) at 2.97 eV (417.5 nm). This response is ascribed to the electronic absorption at 6.03 eV (205.6 nm) with vertical excitation (Figure S7a). On the other hand, the strongest SHG response (about $67\,000.0 \times 10^{-30}$ esu) at 2.21 eV (561.1 nm) of (4,4) BCNNT *e* is much weaker (Figure S9). In the OR process (Figure 3h), there are two strong responses, one (over $3.0 \times 10^{10} \times 10^{-30}$ esu) at 3.62 eV (342.5 nm) and the other one (over $1.0 \times 10^{10} \times 10^{-30}$ esu) at 4.24 eV (292.5 nm). Charge transfer based electronic excitations (Figure S7b) contribute to the strong OR response at 3.62 eV. The OR response of (4,4) BCNNT *e* is much weaker (about $4.0 \times 10^{6} \times 10^{-30}$ esu) at 4.42 eV (280.5 nm), or about 4 orders of magnitude smaller than that of (8,0) BCNNT *e*.

(8,0) BCNNT f. The saturation of carbon atoms in (8,0) BCNNT *f* [$B_{56}N_{56}C_{48}H_{64}$(8,0)-exo, with hydrogen atoms bonded to the outside of the tube] disrupts the π conjugation of the tube. This BCNNT has roughly similar electronic spectra to those of BNNT *b*. This is also the case for the second-order NLO responses. In the SHG process (Figure 3i), BCNNT *f* has two relatively strong responses at 3.44 eV (360.0 nm) and 3.63 eV (341.5 nm). The response (over $2.8 \times 10^{4} \times 10^{-30}$ esu) at 3.44 eV is mainly ascribed to the short-range charge transfer based excitation at 6.63 eV (187.0 nm) (Figure S10a). The response of OR increases monotonically with the strength of the external field, as shown in Figure S10b.

(8,0) BCNNT g. The bonding of one hydrogen atom to carbon inside the nanotube has a slight effect on the electronic structure of (8,0) BCNNT *g* in comparison with that of (8,0) BCNNT *f*; for example, the position of absorption peaks and the related oscillator strengths change slightly. This in turn leads to different NLO responses to external fields, as shown in Figure 3j. The strongest SHG response (about $8.0 \times 10^{4} \times 10^{-30}$ esu) of (8,0) BCNNT *g* occurs at 3.27 eV (379.0 nm), and the other one (about $2.0 \times 10^{4} \times 10^{-30}$ esu) occurs at 3.53 eV (351.2 nm). The monotonic increase of the OR response with the strength of the external field in (8,0) BCNNT *g* (Figure S11b) is similar to that of (8,0) BCNNT *f*.

In summary, the BCNNTs with different doping patterns have different second-order NLO responses to external fields. The alternately doped (8,0) BCNNTs (*d* and *e*) have the largest NLO responses. The hydrogenated (8,0) BCNNTs (*f* and *g*) have the smallest responses. (8,0) BCNNT *d*, doped with two layers of carbon circles, is the best candidate for application in second-harmonic generation in the visible region around 440.0 nm. (8,0) BCNNT *e*, alternately doped with a single carbon circle, is suitable for application in optical rectification in the region close to the visible region around 330.0 nm. The strong response of (8,0) BCNNT *c* (half/half graft) from infrared to visible regions in the SHG process suggests its potential application. Although the NLO responses of (4,4) BCNNTs are much smaller than their corresponding (8,0) BCNNTs, the effect of carbon doping on the NLO properties of BNNT is clearly revealed in the (4,4) BCNNTs.

However, as the length of the nanotube increases, the edge effect from the open ends of the tube might diminish. In such cases, the junction between carbon cycle and BN cycle could play an important role in NLO properties. An edge effect is significant in BN-doped carbon nanotubes[27] and short N-doped carbon nanotubes.[52]

CONCLUSIONS

The unfavorable bonding between carbon and boron (or nitrogen), with respect to that between boron and nitrogen (and between carbon atoms), destabilizes the alternately doped BCNNTs and brings about localized charge distribution and charge polarization. It is energetically more favorable for the doping carbon circles in zigzag BNNTs than that in armchair BNNTs. The doping of carbon cycles in BNNT combines the properties of both carbon nanotube and BNNT and leads to low-energy electronic excitations.

The strong second-order NLO responses in the low-energy field (visible and infrared) make these hybrid nanotubes potential NLO materials for application in these regions. The doping pattern and π conjugation in these nanotubes play crucial roles in determining the NLO optical properties of these hybrid nanotubes.

ASSOCIATED CONTENT

Supporting Information

Atomic charge, electronic spectra, evolution of the static first hyperpolarizability with the electronic spectra, relevant molecular orbitals involved in the electronic excitations with significant contributions to the static first hyperpolarizability, and the nature of major electronic excitations of (8,0) BNNT and BCNNTs. The evolution of the static first hyperpolarizability with the electronic spectra of (4,4) BNNT and BCNNTs. This material is available free of charge via the Internet at http://pubs.acs.org.

AUTHOR INFORMATION

Corresponding Authors

*E-mail: tccliweiqi@hit.edu.cn.
*E-mail: tianwq@hit.edu.cn.

Notes

The authors declare no competing financial interest.

ACKNOWLEDGMENTS

This work is supported by Nature Science Foundation of China (11104048), the State Key Lab of Urban Water Resource and Environment (HIT) (2014TS01), and the Open Project of State Key Laboratory of Supramolecular Structure and Materials (JLU) (SKLSSM201404). The critical reading and constructive comments from the reviewers are gratefully appreciated.

REFERENCES

(1) de la Torre, G.; Vázquez, P.; Agulló-López, F.; Torres, T. Role of structural factors in the nonlinear optical properties of phthalocyanines and related compounds. *Chem. Rev.* **2004**, *104*, 3723−3750.

(2) Coe, B. J.; Harris, J. A.; Brunschwig, B. S.; Asselberghs, I.; Clays, K.; Garin, J.; Orduna, J. Three-dimensional nonlinear optical chromophores based on metal-to-ligand charge-transfer from ruthenium(II) or iron(II) centers. *J. Am. Chem. Soc.* **2005**, *127*, 13399−13410.

(3) Klein, M. B.; Dunning, G. J.; Valley, G. C.; Lind, R. C.; O'Meara, T. R. Imaging threshold detector using a phase-conjugate resonator in $BaTiO_3$. *Opt. Lett.* **1986**, *11*, 575−577.

(4) Hou, H. W.; Wei, Y. L.; Song, Y. L.; Mi, L. W.; Tang, M. S.; Li, L. K.; Fan, Y. T. Metal ions play different roles in the third-order

nonlinear optical properties of d^{10} metal−organic clusters. *Angew. Chem., Int. Ed.* **2005**, *44*, 6067−6074.
(5) Chen, X. H.; Wu, K. C.; Snijders, J. G.; Lin, C. S. Electronic structures and nonlinear optical properties of trinuclear transition metal clusters M−(μ-S)−M′ (M = Mo, W; M′ = Cu, Ag, Au). *Inorg. Chem.* **2003**, *42*, 532−540.
(6) Nie, W. Optical nonlinearity: phenomena, applications, and materials. *Adv. Mater.* **1993**, *5*, 520−545.
(7) Brédas, J. L.; Adant, C.; Tackx, P.; Persoons, A.; Pierce, B. M. Third-order nonlinear optical response in organic materials: theoretical and experimental aspects. *Chem. Rev.* **1994**, *94*, 243−278.
(8) Di Bella, S. Second-order nonlinear optical properties of transition metal complexes. *Chem. Soc. Rev.* **2001**, *30*, 355−366.
(9) Lacroix, P. G. Second-order optical nonlinearities in coordination chemistry: the case of bis(salicylaldiminato)metal Schiff base complexes. *Eur. J. Inorg. Chem.* **2001**, *2*, 339−348.
(10) Coe, B. J. Switchable nonlinear optical metallochromophores with pyridinium electron acceptor groups. *Acc. Chem. Res.* **2006**, *39*, 383−393.
(11) Kanis, D. R.; Ratner, M. A.; Marks, T. J. Design and construction of molecular assemblies with large second-order optical nonlinearities, quantum chemical aspects. *Chem. Rev.* **1994**, *94*, 195−242.
(12) Wildöer, J. W. G.; Venema, L. C.; Rinzler, A. G.; Smalley, R. E.; Dekker, C. Electronic structure of atomically resolved carbon nanotubes. *Nature* **1998**, *391*, 59−62.
(13) Barone, V.; Scuseria, G. E. Theoretical study of the electronic properties of narrow single-walled carbon nanotubes: beyond the local density approximation. *J. Chem. Phys.* **2004**, *121*, 10376−10379.
(14) Blasé, X.; Rubio, A.; Louie, S. G.; Cohen, M. L. Stability and band-gap constancy of boron-nitride nanotubes. *Europhys. Lett.* **1994**, *28*, 335−340.
(15) Rubio, A.; Corkill, J. L.; Cohen, M. L. Theory of graphitic boron nitride nanotubes. *Phys. Rev. B* **1994**, *49*, 5081−5084.
(16) Chopra, N. G.; Luyken, R. J.; Cherrey, K.; Crespi, V. H.; Cohen, M. L.; Louie, S. G.; Zettl, A. Boron nitride nanotubes. *Science* **1995**, *269*, 966−967.
(17) Baughman, R. H.; Zakhidov, A. A.; de Heer, W. A. Carbon nanotubes-the route toward applications. *Science* **2002**, *297*, 787−792.
(18) Terrones, M.; Romo-Herrera, J. M.; Cruz-Silva, E.; López-Urías, F.; Muñoz-Sandoval, E.; Velázquez-Salazar, J. J.; Terrones, H.; Bando, Y.; Golberg, D. Pure and doped boron nitride nanotubes. *Mater. Today* **2007**, *10*, 30−38.
(19) Golberg, D.; Bando, Y.; Tang, C. C.; Zhi, C. Y. Boron nitride nanotubes. *Adv. Mater.* **2007**, *19*, 2413−2432.
(20) Wang, W. L.; Bai, X. D.; Liu, K. H.; Xu, Z.; Golberg, D.; Bando, Y.; Wang, E. G. Direct synthesis of B-C-N single-walled nanotubes by bias-assisted hot filament chemical vapor deposition. *J. Am. Chem. Soc.* **2006**, *128*, 6530−6531.
(21) Enouz, S.; Stéphan, O.; Cochon, J. L.; Colliex, C.; Loiseau, A. C-BN patterned single-walled nanotubes synthesized by laser vaporization. *Nano Lett.* **2007**, *7*, 1856−1862.
(22) Enouz-Védrenne, S.; Stéphan, O.; Glerup, M.; Cochon, J. L.; Colliex, C.; Loiseau, A. Effect of the synthesis method on the distribution of C, B, and N elements in multiwall nanotubes: a spatially resolved electron energy loss spectroscopy study. *J. Phys. Chem. C* **2008**, *112*, 16422−16430.
(23) Zhang, Z. Y.; Zhang, Z. H.; Guo, W. L. Stability and electronic properties of a novel C-BN heteronanotube from first-principles calculations. *J. Phys. Chem. C* **2009**, *113*, 13108−13114.
(24) Du, A. J.; Chen, Y.; Zhu, Z. H.; Lu, G. Q.; Smith, S. C. C-BN single-walled nanotubes from hybrid connection of BN/C nanoribbons: prediction by *ab initio* density functional calculations. *J. Am. Chem. Soc.* **2009**, *131*, 1682−1683.
(25) Pan, H.; Feng, Y. P.; Lin, J. Y. *Ab initio* study of single-wall BC_2N nanotubes. *Phys. Rev. B* **2006**, *74*, 045409 (1−4).
(26) Guo, G. Y.; Lin, J. C. Second-harmonic generation and linear electro-optical coefficients of BN nanotubes. *Phys. Rev. B* **2005**, *72*, 075416 (1−9)..
(27) Zhong, R. L.; Sun, S. L.; Xu, H. L.; Qiu, Y. Q.; Su, Z. M. BN segment doped effect on the first hyperpolarizability of heteronanotubes: focused on an effective connecting pattern. *J. Phys. Chem. C* **2013**, *117*, 10039−10044.
(28) Orlando, R.; Bast, R.; Ruud, K.; Ekström, U.; Ferrabone, M.; Kirtman, B.; Dovesi, R. The first and second static electronic hyper polarizabilities onf zigzag boron nitride nanotubes. An ab initio approach through the coupled perturbed Kohn-Sham scheme. *J. Phys. Chem. A* **2011**, *115*, 12631−12637.
(29) Zhong, R. L.; Xu, H. L.; Sun, S. L.; Qiu, Y. Q.; Su, Z. M. The excess electron in a boron nitride nanotube: pyramidal NBO charge distribution and remarkable first hyperpolarizability. *Chem.—Eur. J.* **2012**, *18*, 11350−11355.
(30) Chen, W.; Yu, G. T.; Gu, F. L.; Aoki, Y. Investigation on the electronic structures and nonlinear optical properties of pristine boron nitride and boron nitride-carbon heterostructured single-wall nanotubes by the elongation method. *J. Phys. Chem. C* **2009**, *113*, 8447−8454.
(31) Liu, Z.; Ma, L.-L.; Shi, G.; Zhou, W.; Gong, Y.-J.; Lei, S.-D.; Yang, X.-B.; Zhang, J.-N.; Yu, J.-J.; Hackenberg, K. P.; Babakhani, A.; Idrobo, J.-C.; Vajtai, R.; Lou, J.; Ajayan, P. M. In-plane heterostructures of graphene and hexagonal boron nitride with controlled domain sizes. *Nat. Nanotechnol.* **2013**, *8*, 119−124.
(32) Hohenberg, P.; Kohn, W. Inhomogeneous electron gas. *Phys. Rev.* **1964**, *136*, B864−B871.
(33) Kohn, W.; Sham, L. J. Self-consistent equations including exchange and correlation effects. *Phys. Rev.* **1965**, *140*, A1133−A1138.
(34) Parr, R. G.; Yang, W. *Density-Functional Theory of Atoms and Molecules*; Oxford University Press: New York, 1989.
(35) Lee, C.; Yang, W.; Parr, R. G. Development of the Colle-Salvetti correlation-energy formula into a functional of the electron density. *Phys. Rev. B* **1988**, *37*, 785−789.
(36) Becke, A. D. Density-functional thermochemistry. III. The role of exact exchange. *J. Chem. Phys.* **1993**, *98*, 5648−5652.
(37) Hehre, W. J.; Ditchfield, R.; Pople, J. A. Self-consistent molecular orbital methods. XII. further extensions of gaussian-type basis sets for use in molecular orbital studies of organic molecules. *J. Chem. Phys.* **1972**, *56*, 2257−2261.
(38) Hariharan, P. C.; Pople, J. A. The influence of polarization functions on molecular orbital hydrogenation energies. *Theor. Chem. Acta* **1973**, *28*, 213−222.
(39) Frisch, M. J.; Trucks, G. W.; Schlegel, H. B.; Scuseria, G. E.; Robb, M. A.; Cheeseman, J. R.; Montgomery, J. A., Jr.; Vreven, T.; Kudin, K. N.; Burant, J. C.; Millam, J. M.; Iyengar, S. S.; Tomasi, J.; Barone, V.; Mennucci, B.; Cossi, M.; Scalmani, G.; Rega, N.; Petersson, G. A.; Nakatsuji, H.; Hada, M.; Ehara, M.; Toyota, K.; Fukuda, R.; Hasegawa, J.; Ishida, M.; Nakajima, T.; Honda, Y.; Kitao, O.; Nakai, H.; Klene, M.; Li, X.; Knox, J. E.; Hratchian, H. P.; Cross, J. B.; Bakken, V.; Adamo, C.; Jaramillo, J.; Gomperts, R.; Stratmann, R. E.; Yazyev, O.; Austin, A. J.; Cammi, R.; Pomelli, C.; Ochterski, J. W.; Ayala, P. Y.; Morokuma, K.; Voth, G. A.; Salvador, P.; Dannenberg, J. J.; Zakrzewski, V. G.; Dapprich, S.; Daniels, A. D.; Strain, M. C.; Farkas, O.; Malick, D. K.; Rabuck, A. D.; Raghavachari, K.; Foresman, J. B.; Ortiz, J. V.; Cui, Q.; Baboul, A. G.; Clifford, S.; Cioslowski, J.; Stefanov, B. B.; Liu, G.; Liashenko, A.; Piskorz, P.; Komaromi, I.; Martin, R. L.; Fox, D. J.; Keith, T.; Al-Laham, M. A.; Peng, C. Y.; Nanayakkara, A.; Challacombe, M.; Gill, P. M. W.; Johnson, B.; Chen, W.; Wong, M. W.; Gonzalez, C.; Pople, J. A. *Gaussian 03*, Revision E.01; Gaussian, Inc.: Wallingford, CT, 2004.
(40) Ridley, J. E.; Zerner, M. C. Triplet states via intermediate neglect of differential overlap: benzene, pyridine and the diazines. *Theor. Chem. Acta* **1976**, *42*, 223−236.
(41) Orr, B. J.; Ward, J. F. Perturbation theory of the non-linear optical polarization of an isolated system. *Mol. Phys.* **1971**, *20*, 513−526.
(42) Bishop, D. M. Explicit nondivergent formulas for atomic and molecular dynamic hyperpolarizabilities. *J. Chem. Phys.* **1994**, *100*, 6535−6542.

(43) Feng, J. K.; Gao, X. L.; Li, J.; Sun, J. Z. Quantum-mechanical study on nonlinear 2nd-order optical susceptibilities. *Chin. Sci. Bull.* **1990**, *35*, 2022−2023.
(44) Tian, W. Q. Modeling nonlinear optics of nanosystems with sum-over-states model. *J. Comput. Chem.* **2012**, *33*, 466−470.
(45) Hu, Y. Y.; Sun, S. L.; Tian, W. T.; Tian, W. Q.; Xu, H. L.; Su, Z. M. Influence of spiral framework on nonlinear optical materials. *ChemPhysChem* **2014**, *15*, 929−934.
(46) Gieseking, R. L.; Mukhopadhyay, S.; Risko, C.; Brédas, J.-L. Impact of the nature of the excited-state transition dipole moments on the third-order nonlinear optical response of polymethine dyes for all-optical switching applications. *ACS Photonics* **2014**, *1*, 261−269 and references therein.
(47) Brothers, E. N.; Scuseria, G. E.; Kudin, K. N. Longitudinal polarizability of carbon nanotubes. *J. Phys. Chem. B* **2006**, *110*, 12860−12864.
(48) Demichelis, R.; Noël, R.; D'Arco, P.; Rérat, M.; Claudio, M.; Zicovich-Wilson, C. M.; Dovesi, R. Properties of carbon nanotubes: an ab initio study using large gaussian basis sets and various DFT functionals. *J. Phys. Chem. C* **2011**, *115*, 8876−8885.
(49) Hod, O.; Scuseria, G. E. Half-metallic zigzag carbon nanotube dots. *ACS Nano* **2008**, *2*, 2243−2249.
(50) Zhou, X.; Li, W.-Q.; Shao, B.; Tian, W. Q. Nonlinear optic properties of fullerene $C_{96}(D_{3d})$ and related heterofullerenes. *J. Phys. Chem. C* **2013**, *117*, 23172−23177.
(51) Margulis, Vl. A.; Muryumin, E. E.; Gaiduk, E. A. Second-order nonlinear optical response of zigzag BN single-walled nanotubes. *Phys. Rev. B* **2010**, *82*, 235426 (1−18).
(52) Xu, H. L.; Wang, F. F.; Li, Z. R.; Wang, B. Q.; Wu, D.; Chen, W.; Yu, G. T.; Gu, F. L.; Aoki, Y. The nitrogen edge-doped effect on the static first hyperpolarizability of the supershort single-walled carbon nanotube. *J. Comput. Chem.* **2009**, *30*, 1128−1134.